View metadata, citation and similar papers at core.ac.uk

brought to you by CORE

provided by Syracuse University Research Facility and Collaborative Environment

Syracuse University

SURFACE at Syracuse University

Physics

College of Arts and Sciences

4-29-2016

Electron and hole drift mobility measurements on methylammonium lead iodide perovskite solar cells

Brian Maynard

Qi Long

Eric A. Schiff
Syracuse University

Mengjin Yang

Kai Zhu

See next page for additional authors

Follow this and additional works at: https://surface.syr.edu/phy

 Part of the Physics Commons

Recommended Citation

B Maynard, Q Long, E Schiff, M Yang, K Zhu, R Kottokkaran, H Abbas, V Dalal (2016) Electron and hole drift mobility measurements on methylammonium lead iodide perovskite solar cells; DOI: https://doi.org/10.1063/1.4948344; AIP

This Manuscript is brought to you for free and open access by the College of Arts and Sciences at SURFACE at Syracuse University. It has been accepted for inclusion in Physics by an authorized administrator of SURFACE at Syracuse University. For more information, please contact surface@syr.edu.

Author(s)/Creator(s)
Brian Maynard, Qi Long, Eric A. Schiff, Mengjin Yang, Kai Zhu, Ranjith Kottokkaran, Hisham Abbas, and Vikram L. Dalal

This manuscript is available at SURFACE at Syracuse University: https://surface.syr.edu/phy/530

AIP | Applied Physics Letters

Electron and hole drift mobility measurements on methylammonium lead iodide perovskite solar cells

Brian Maynard, Qi Long, Eric A. Schiff, Mengjin Yang, Kai Zhu, Ranjith Kottokkaran, Hisham Abbas, and Vikram L. Dalal

Citation: Applied Physics Letters **108**, 173505 (2016); doi: 10.1063/1.4948344
View online: http://dx.doi.org/10.1063/1.4948344
View Table of Contents: http://scitation.aip.org/content/aip/journal/apl/108/17?ver=pdfcov
Published by the AIP Publishing

Articles you may be interested in

Parameters influencing the deposition of methylammonium lead halide iodide in hole conductor free perovskite-based solar cells
APL Mater. **2**, 081502 (2014); 10.1063/1.4885548

Persistent photovoltage in methylammonium lead iodide perovskite solar cells
APL Mater. **2**, 081501 (2014); 10.1063/1.4885255

Electron and hole drift mobility measurements on thin film CdTe solar cells
Appl. Phys. Lett. **105**, 042106 (2014); 10.1063/1.4891846

Electron drift-mobility measurements in polycrystalline CuIn1−xGaxSe2 solar cells
Appl. Phys. Lett. **100**, 103901 (2012); 10.1063/1.3692165

The effect of carrier mobility in organic solar cells
J. Appl. Phys. **107**, 084503 (2010); 10.1063/1.3327210

Reuse of AIP Publishing content is subject to the terms at: https://publishing.aip.org/authors/rights-and-permissions. Download to IP: 205.254.147.8 On: Fri, 29 Apr 2016 15:50:19

Electron and hole drift mobility measurements on methylammonium lead iodide perovskite solar cells

Brian Maynard,[1] Qi Long,[1] Eric A. Schiff,[1] Mengjin Yang,[2] Kai Zhu,[2] Ranjith Kottokkaran,[3] Hisham Abbas,[3] and Vikram L. Dalal[3]
[1]*Department of Physics, Syracuse University, Syracuse, New York 13244, USA*
[2]*National Renewable Energy Laboratory, Golden, Colorado 80401, USA*
[3]*Iowa State University, Ames, Iowa 50011, USA*

(Received 27 January 2016; accepted 17 April 2016; published online 29 April 2016)

We report nanosecond domain time-of-flight measurements of electron and hole photocarriers in methylammonium lead iodide perovskite solar cells. The mobilities ranged from 0.06 to 1.4 cm^2/Vs at room temperature, but there is little systematic difference between the two carriers. We also find that the drift mobilities are dispersive (time-dependent). The dispersion parameters are in the range of 0.4–0.7, and they imply that terahertz domain mobilities will be much larger than nanosecond domain mobilities. The temperature-dependences of the dispersion parameters are consistent with confinement of electron and hole transport to fractal-like spatial networks within nanoseconds of their photogeneration. *Published by AIP Publishing.*
[http://dx.doi.org/10.1063/1.4948344]

The achievement of solar conversion efficiencies exceeding 20% in perovskite solar cells has been remarkably rapid,[1] and little can yet be said definitively of the interplay between photocarrier generation, transport, and recombination processes that have enabled it. Among the crucial, poorly known materials, parameters are drift mobilities. Larger minority carrier mobilities play a direct role in solar cells by increasing their useful thickness and hence their photocurrent.[2] They play a subtler role for the open-circuit voltage. When photocarrier recombination occurs on defects such as grain boundaries, lower mobilities and reduced rates of diffusion-limited recombination can increase the open-circuit voltage.[3,4] For a methylammonium lead iodide ($MAPbI_3$) perovskite single crystal, the reported hole drift-mobility is more than 100 cm^2/Vs.[5] For $MAPbI_3$ thin films similar to those used in high-efficiency solar cells, mobilities have been estimated using a variety of techniques. The mobilities spread over a large range from 10^{-4} to 10 cm^2/Vs.[6–10]

In this letter, we present drift mobility measurements for $MAPbI_3$ thin film solar cells from two laboratories. We use the canonical photocarrier time-of-flight (TOF) technique,[11] which has not been fully implemented in previous work. As a consequence, we clearly distinguish electron and hole mobilities. They are in the range of 0.06–1.4 cm^2/Vs under standard conditions, with little systematic difference between them. A second finding is that both drift mobilities are dispersive, which means that the drift mobility gets smaller as the delay since photogeneration increases.[12] Dispersion is a well-known effect in low-mobility materials but has not been reported in perovskites. Based on the temperature-dependence measurements we report here, we think the dispersion parameter in perovskites is a structural parameter reflecting the confinement of photocarriers to fractal-like paths.

Sample properties are summarized in Table I. One coupon is from Iowa State University (ISU), and two coupons are from the National Renewable Energy Laboratory (NREL). The ISU samples are superstrate n-i-p cells with the structure glass/fluorine doped tin oxide (FTO)/TiO_2/$MAPbI_3$/poly(3-hexyl)thiophene (P3HT)/Au.[13] The NREL samples have the same structure excepting the use of 2,2′,7,7′-Tetrakis[N,N-di(4-methoxyphenyl)amino]-9,9′-spirobifluorene (spiro-MeOTAD)/Ag for the back contacts.[14] Some additional cell preparation information is presented in supplementary material.[15] Sample capacitances were measured in conjunction with the time-of-flight measurement. We used the capacitance to estimate the thickness of the $MAPbI_3$ layer using a previously reported relative dielectric constant of 18;[13] we confirmed that this measurement gave an absorber thickness consistent with SEM and profilometer results.[15] We minimized air exposure of the samples to avoid deterioration, which we monitored using the open-circuit voltage V_{OC} measured using a solar simulator. Over the course of the measurements reported here, V_{OC} declined by less than 0.05 V.

Photocarrier time-of-flight (TOF) measures the transit time t_T for an initial distribution of photocarriers to be displaced a distance L by an electric field E; the drift-mobility is then defined as $\mu_D = L/(Et_T)$.[16] For our TOF measurements, we generated photocarriers with an illumination pulse (about 10 ns) from a diode laser emitting at a wavelength of 660 nm. A bias voltage was applied to the cell 20 μs before the laser pulse; the current transient in the bias circuit was integrated to determine the capacitance, and the laser pulse was incident through the glass substrate. The front TiO_2 transport layer is transparent at 660 nm and has a sufficient dark conductivity that we do not expect it contribute to the photocurrents. We estimate the absorption depth at 660 nm to be about 0.2 μm in the $MAPbI_3$ layer,[17] which is significantly less than the thicknesses of the absorber layers of the cell.

The left panel of Fig. 1 shows the corresponding photocharge transients in one cell for both reverse and forward bias voltages; we actually record the transient photocurrent

Reuse of AIP Publishing content is subject to the terms at: https://publishing.aip.org/authors/rights-and-permissions. Download to IP: 205.254.147.8 On: Fri, 29 Apr 2016 15:50:19

TABLE I. Sample properties at room temperature. Sample codes—I: Iowa State University and N: National Renewable Energy Laboratory. Mobilities and dispersion parameters correspond to the displacement-field ratio $L/E = 10^{-8}$ cm^2/V.

Sample	Thickness (μm)	V_{OC} (V)	μ_h (cm^2/Vs)	α_h	$\mu\tau_h$ (cm^2/V)	μ_e (cm^2/Vs)	α_e	$\mu\tau_e$ (cm^2/V)
I3B1	1.20	0.62	0.23	0.71	1.3×10^{-7}	1.4	0.57	1.8×10^{-7}
I3B2	1.20	0.65	0.40	0.74	1.3×10^{-7}	…	…	…
N3C3	0.80	0.90	0.14	…	2.0×10^{-8}	0.063	…	2.0×10^{-8}
N4C3	0.89	1.00	0.063	0.40	3.0×10^{-8}	0.11	0.43	4.0×10^{-8}

in the voltage bias circuit and calculate the charge by integrating. Photocurrents under reverse bias are mostly due to holes and under forward bias are mostly due to electrons. It is unusual in time-of-flight experiments with solar cells to measure transients under forward bias as large as 0.8 V. For our cells, this was possible because the large steady-state dark currents are not established for hundreds of microseconds after the application of the forward bias. The applied field across the absorber layer thus remained uniform long enough for the time-of-flight measurement to be concluded. We have not attempted further modeling of these double-injection current transients. Other materials also exhibit substantial delays in their onset, and in principle, they can be used to infer drift mobilities.[18]

The right panel of Fig. 1 shows the photocharge collected in 3 μs at the different voltages. For voltages $V < -0.3$ V, the photocharge collection is fairly constant around 14 pC, which corresponds to the charge Q_0 of holes from the initial laser pulse. The photocharge of -14 pC for voltages $V > +0.3$ V corresponds to the photogenerated electrons. For smaller voltage magnitudes, charge collection is incomplete, which we attribute to "deep trapping" by unknown defects. The dashed lines in the right panel are fits to the Hecht formula for deep-trapping,[19] which yield the deep-trapping mobility-lifetime products $\mu\tau_h$ and $\mu\tau_e$, respectively. The intercept V_0, where the collected charge is zero, is determined by the built-in electric field averaged across the initial photocarrier distribution. V_0 is much less than the open-circuit voltages (and hence the built-in potentials) of the cells. This suggests that there is a region with a much larger built-in field near the front TiO_2/$MAPbI_3$ contact of the cells. This conclusion is reasonably consistent with direct field profiling on similar samples.[20]

The sections of the photocharge transients rising from $t = 0$ in the left panel of Fig. 1 are used to obtain the "half-collection transit times" from the intersections with the half-collection ($Q = Q_0/2 = 7$ pC) line. The corresponding displacement of the mean position of the photocharge distribution since photogeneration is $d/2$, where d is the thickness of the absorber layer. In the lower panel of Fig. 2, we illustrate the process of determining the transit time in more detail using two transients, the sample used for Fig. 1 (ISU) and a second NREL sample. The two transients were selected to have the same risetimes; both reach their half-charge levels ($Q/Q_0 = 0.5$) at about 140 ns. The transit time was calculated with a correction for the ultimate risetime RC of our apparatus, which is the product of the capacitance C of the cell and impedance R due to the 50 Ohm electronics.[21] Thus, $t_T = 130$ ns for the ISU sample. We define the drift mobility in terms of this half-collection transit time

$$\mu_D = d^2/(2|V_0 - V|t_T), \tag{1}$$

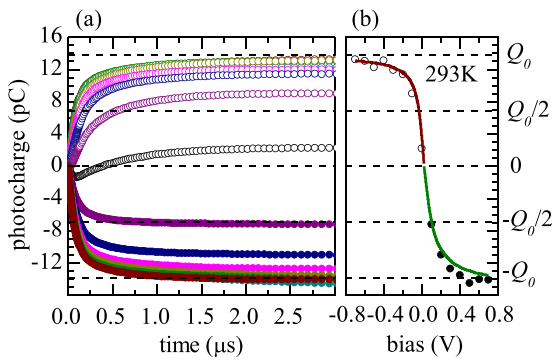

FIG. 1. (Left) Photocharge transients following a laser diode pulse; the different transients correspond to varying bias voltages for sample I3B1 at $T = 293$ K. Positive photocharge corresponds to hole motion, and negative photocharge to electron motion. (right) The symbols indicate the photocharge collected at 3 μs for varying bias voltages. The solid curve indicates fittings to the Hecht deep-trapping analysis (total photocharge $Q_0 = 13.8$ pC, $\mu\tau_h = 1.3 \times 10^{-7}$ cm^2/V, $\mu\tau_e = 1.8 \times 10^{-7}$ cm^2/V, $V_0 = 0.022$ V).

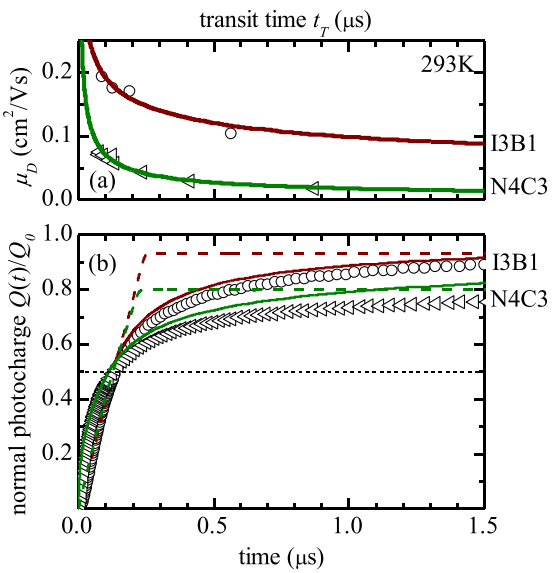

FIG. 2. (Lower) The symbols represent the photocharge transients for two samples after normalization by the total photocharge Q_0 determined by Hecht analysis. The transients were selected to have nearly the same transit times as determined from the intersection with the $Q(t)/Q_0 = 0.5$ line (-0.3 V I3 and -0.25 V N4). The dashed lines are calculated using non-dispersive transport including deep-trapping and at the same common transit time of 130 ns. The solid lines are calculations using the dispersion parameters obtained from the upper panel, neglecting deep-trapping, and with the common transit time. (Upper) The symbols represent drift mobility estimates for the two samples at varying transit times (and bias voltages). The solid lines are best fits using the dispersive model ($\alpha = 0.71$ for I3B1, $\alpha = 0.40$ for N4C3).

Reuse of AIP Publishing content is subject to the terms at: https://publishing.aip.org/authors/rights-and-permissions. Download to IP: 205.254.147.8 On: Fri, 29 Apr 2016 15:50:19

which yields 0.18 cm^2/Vs for the holes in the ISU sample. For the NREL sample, with a different thickness and V_0 value, the drift mobility is 0.06 cm^2/Vs.

The dashed lines rising nearly to $Q = 1.0$ are calculations of the photocharge transient using the standard semiconductor model in which the initial photocarrier distribution drifts at constant speed through the absorber layer.[21] The measured photocharge is then roughly proportional to time until the photocarriers reach the back contact. The half-collection transit time was fitted to match the experimental measurement. The calculated lines also include deep-trapping using the full Hecht calculation, which is why the final collection at these voltages is less than Q_0. As can be seen, this model fits the measured transients poorly.

One extension of mobility models is "dispersion," for which the average speed of the photocarrier distribution falls as the distribution "ages" following photogeneration.[12] We will discuss some physical mechanisms for dispersion shortly. In the top panel of Fig. 2, we show the hole drift mobilities calculated from transients at different voltages for both samples; as can be seen, their magnitudes decline with larger transit times. We also show fits to a dispersive transport formula

$$\mu_D = \frac{\mu_0}{\alpha}(\nu t_T)^{\alpha-1}, \tag{2}$$

where α is the dispersion parameter with a value between 0 and 1.[22] μ_0 is the drift mobility at times of order $1/\nu$. The ISU and NREL sample measurements are fit well using $\alpha = 0.71$ and 0.40, respectively. At shorter times, mobilities get significantly larger. The hole drift mobility of N4C3 is about 0.06 cm^2/Vs at 10^{-7} s; at 10^{-12} s, in the terahertz domain, the dispersion parameter of 0.4 yields a drift mobility of 60 cm^2/Vs. Large majority carrier mobilities have been estimated in perovskite films using absolute measurements of terahertz transmittance.[7]

Returning to the bottom panel, the solid lines are fits to the photocharge transients using the expressions for a dispersive photocharge transient from Ref. 22 and the dispersion parameters just noted. Deep trapping is not included in the calculation with dispersion, and the measurements are noticeably lower than the fitting curve for the NREL sample. Nonetheless, we consider the fittings sufficient to be conclusive support for dispersion.

In Table I, we have summarized the sample properties we have measured at room temperature. These include the open-circuit voltages V_{OC} measured using a solar simulator, and the time-of-flight drift mobilities, dispersion parameters, and deep-trapping mobility-lifetime products for electrons and holes. With dispersive transport, comparing mobilities in different samples must be done at a definite ratio $L/E = d^2/(2|V_0 - V|)$ of the photocarrier displacement L and the electric field E.[16] For the present work on perovskite cells, we have found that $L/E = 10^{-8}$ cm^2/V works well. We estimated the drift mobilities in the table by interpolating between measured values at varying voltages. As illustrated by the fits in the top panel of Fig. 2, estimating a dispersion parameter requires that there be a significant "window" of transit times; at short times, our measurements are limited by the *RC* risetime, and at long times by deep-trapping. For a few cases, this window was inadequate to permit us to estimate dispersion parameters.

The low mobilities in Table I may seem surprising in the context of the excellent photocarrier conversion efficiencies for champion perovskite solar cells. For low-mobility solar cells, the useful thickness of a cell can be roughly estimated from the minority-carrier drift-mobility, which causes a space-charge effect in a cell under solar illumination. The calculation shows that mobilities in the range of 0.1–1.0 cm^2/Vs correspond to an optimum thickness below 1 μm, 2 which is consistent with the $MAPbI_3$ thicknesses in champion cells. Low mobilities are advantageous to the open-circuit voltage when photocarrier recombination occurs on grain boundaries or other microscopic features, since recombination times are lengthened when diffusion to these features is slowed. This possibility may explain why thin-film, low-mobility polycrystalline solar cells such as perovskites and CdTe can have excellent solar conversion efficiencies.

What physical mechanisms can explain the lowered mobilities and dispersion in polycrystalline thin film perovskite layers? The best-known physical mechanism for dispersion is "exponential bandtail multiple trapping" in amorphous semiconductors. In this mechanism, photocarriers are trapped and released by localized electronic states lying close to the band edge energy that divides the traps and delocalized transport states. Band tails are a consequence of disorder in chemical bonding that is expected for non-crystalline solids.[23] This mechanism yields a dispersion parameter that's proportional to absolute temperature; the proportionality constant is determined by the width of the bandtail.[16] The mechanism can be excluded for the perovskite cells that we studied by the temperature-dependent measurements in Fig. 3, which show that the dispersion parameters in the perovskite samples have much weaker (if any) temperature dependence.

Weakly temperature-dependent dispersive transport has been reported several times over the years. This includes holes in polyvinylcarbazole (PVK),[24] electrons in poly(p-phenylene vinylene) (PPV),[25] electrons and holes

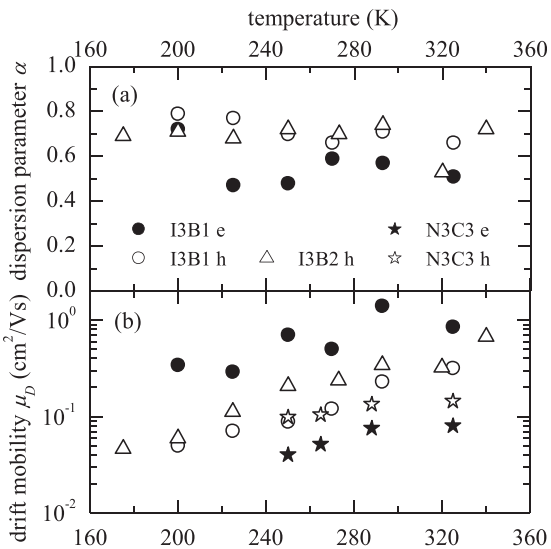

FIG. 3. Temperature dependence measurements for the dispersion parameters and drift mobilities of electrons and holes for several samples; e refers to electrons and h to holes. The displacement-field ratio is $L/E = 1 \times 10^{-8}$ cm^2/V.

Reuse of AIP Publishing content is subject to the terms at: https://publishing.aip.org/authors/rights-and-permissions. Download to IP: 205.254.147.8 On: Fri, 29 Apr 2016 15:50:19

in nanoporous silicon,[26] electrons in the organic semiconductor tris(8-Hydroxyquinoline) Aluminum (Alq3),[27] and electrons in sintered TiO_2 nanoparticle aggregates (in dye-sensitized solar cells).[28] These results have been speculatively attributed to "spatial disorder,"[29] which means that the photocarriers are effectively confined to a tortuous path on the length scales probed by the experiment (about 50–100 nm for the present time-of-flight measurements). It is known that diffusion on a random fractal structure is dispersive with a dispersion parameter related to the fractal dimensions of the structure.[30] A generalized Einstein relation then yields the dispersive drift mobility for this model. Porous silicon is the material that offers the most direct illustration of dispersion as a structural parameter for a semiconductor, since small angle X-ray studies of its highly porous structures have indicated a fractal-like arrangement of the mass.[31] In the perovskite thin films, small ferroelectric domains have been measured, and it has been suggested that these domains create the underlying topology for carrier transport.[32] A fractal transport topology would be a further step for this model.

If dispersive transport reflects underlying mesoscopic structural disorder, or fractal dimensions, one might expect that the dispersion parameters for electrons and holes would be the same. For porous silicon, the dispersion parameters of electrons and holes were essentially the same over a large temperature range.[26] The present results on dispersion are more limited, but for the two samples for which we have a good comparison, there is no conclusive difference in the dispersion parameters of electrons and holes. See supplementary material for fabrication details of the solar cells studied.[15] We have also included a discussion on our choice of performing a photocharge over photocurrent analysis.

This research was partly supported by the National Science Foundation (CBET-1336147 and CBET-1336134).

[1]M. A. Green, K. Emery, Y. Hishikawa, W. Warta, and E. D. Dunlop, Prog. Photovoltaics **23**, 1 (2015).
[2]E. A. Schiff, Sol. Energy Mater. Sol. Cells **78**, 567–595 (2003).
[3]D. R. Wight, I. D. Blenkinsop, W. Harding, and B. Hamilton, Phys. Rev. B **23**, 5495 (1981).
[4]M. D. Abbott, R. A. Bardos, T. Trupke, K. C. Fisher, and E. Pink, J. Appl. Phys. **102**, 044502 (2007).
[5]D. Shi, V. Adinolfi, R. Comin, M. Yuan, E. Alarousu, A. Buin, Y. Chen, S. Hoogland, A. Rothenberger, K. Katsiev, Y. Losovyj, X. Zhang, P. A. Dowben, O. F. Mohammed, E. H. Sargent, and O. M. Bakr, Science **347**, 519 (2015).
[6]C. C. Stoumpos, C. D. Malliakas, and M. G. Kanatzidis, Inorg. Chem. **52**, 9019 (2013).
[7]C. Wehrenfennig, G. E. Eperon, M. B. Johnston, H. J. Snaith, and L. M. Herz, Adv. Mater. **26**, 1584 (2014). Subnanosecond photoconductivity transient; magnitude yields about 8 cm^2/Vs. See also T. Leijtens, S. D. Stranks, G. E. Eperon, R. Lindblad, E. M. J. Johansson, I. J. McPherson, H. Rensmo, J. M. Ball, M. M. Lee, and H. J. Snaith, ACS Nano **8**(7), 7147–7155 (2014).
[8]T. J. Savenije, C. S. Ponseca, Jr., L. Kunneman, M. Abdellah, K. Z. Y. Tian, Q. Zhu, S. E. Canton, I. G. Scheblykin, T. Pullerits, A. Yartsev, and V. Sundstroüm, J. Phys. Chem. Lett. **5**, 2189−2194 (2014).
[9]N. Ahn, D.-Y. Son, I.-H. Jang, S. M. Kang, M. Choi, and N.-G. Park, J. Am. Chem. Soc. **137**, 8696−8699 (2015).
[10]Y. Chen, J. Peng, D. Su, X. Chen, and Z. Liang, ACS Appl. Mater. Interfaces **7**, 4471 (2015). CELIV and some TOF (?). CELIV close to 2E-3 near 295 K. EAS—probably erroneous; TOF looks like RC to me.
[11]W. E. Spear, Proc. Phys. Soc. B **70**, 669 (1957).
[12]H. Scher, M. F. Schlesinger, and J. T. Bendler, Phys. Today **44**(1), 26 (1991).
[13]H. Abbas, R. Kottokkaran, M. Samiee, L. Zhang, B. Ganapathy, A. Kitahara, M. Noack, and V. L. Dalal, APL Mater. **3**, 016105 (2015).
[14]Y. Zhou, M. Yang, W. Wu, A. L. Vasiliev, Kai Zhu, and N. P. Padture, J. Mater. Chem. A **3**, 8178 (2015).
[15]See supplementary material at http://dx.doi.org/10.1063/1.4948344 for (i) discussion of sample preparation and thickness and (ii) for a transient photocurrent chart.
[16]Q. Wang, H. Antoniadis, E. A. Schiff, and S. Guha, Phys. Rev. B **47**, 9435 (1993).
[17]S. De Wolf, J. Holovsky, S. J. Moon, P. Loper, B. Niesen, M. Ledinsky, F. J. Haug, J. H. Yum, and C. Ballif, J. Phys. Chem. Lett. **5**, 1035 (2014).
[18]M. Hack and R. A. Street, J. Appl. Phys. **72**, 2331 (1992).
[19]K. Hecht, Z. Phys. **77**, 235 (1932).
[20]C.-S. Jiang, M. Yang, Y. Zhou, B. To, S. U. Nanayakkara, J. M. Luther, W. Zhou, J. J. Berry, J. van de Lagemaat, N. P. Padture, K. Zhu, and M. M. Al-Jassim, Nat. Commun. **6**, 8397 (2015).
[21]S. A. Dinca, E. A. Schiff, B. Egass, R. Noufi, D. L. Young, and W. N. Shafarman, Phys. Rev. B **80**, 235201 (2009).
[22]Q. Long, S. A. Dinca, E. A. Schiff, M. Yu, and J. Theil, Appl. Phys. Lett. **105**, 042106 (2014); see supplementary material.
[23]D. A. Drabold, Y. Li, B. Cai, and M. Zhang, Phys. Rev. B **83**, 045201 (2011).
[24]F. C. Bos, T. Guion, and D. M. Burland, Phys. Rev. B **39**, 12633 (1989).
[25]P. W. M. Blom and M. C. J. M. Vissenberg, Phys. Rev. Lett. **80**, 3819 (1998).
[26]P. N. Rao, E. A. Schiff, L. Tsybeskov, and P. M. Fauchet, Chem. Phys. **284**, 129 (2002).
[27]S. Berleb and W. Brütting, Phys. Rev. Lett. **89**, 286601 (2002).
[28]N. Kopidakis, K. D. Benkstein, J. van de Lagemaat, A. J. Frank, Q. Yuan, and E. A. Schiff, Phys. Rev. B **73**, 045326 (2006).
[29]H. Scher and E. Montroll, Phys. Rev. B **12**, 2455 (1975).
[30]D. ben-Avraham and S. Havlin, *Diffusion and Reactions in Fractals and Disordered Systems* (Cambridge University Press, 2000).
[31]V. Vezin, P. Goudeau, A. Naudon, A. Halimaoui, and G. Bomchil, Appl. Phys. Lett. **60**, 2625 (1992).
[32]Y. Kutes, L. Ye, Y. Zhou, S. Pang, Bryan D. Huey, and N. P. Padture, J. Phys. Chem. Lett. **5**, 3335–3339 (2014).

Reuse of AIP Publishing content is subject to the terms at: https://publishing.aip.org/authors/rights-and-permissions. Download to IP: 205.254.147.8 On: Fri, 29 Apr 2016 15:50:19

Electron and hole drift mobility measurements on methylammonium lead iodide perovskite solar cells

(Supplementary Material)

Brian Maynard[1], Qi Long[1], Eric A. Schiff[1], Mengjin Yang[2], Kai Zhu[2], Ranjith Kottokkaran,[3] Hisham Abbas[3], and Vikram L. Dalal[3]

[1]*Department of Physics, Syracuse University, Syracuse NY 13244, United States*

[2]*National Renewable Energy Laboratory, Golden CO 80401, United States*

[3]*Department of Electrical and Computer Engineering, Iowa State University, Ames IA 50011, United States*

Sample preparation and thickness

The cells used for this work were about 1 μm thick, which is thicker than typical for the highest efficiency perovskite solar cells. Thicker cells are helpful for time-of-flight measurements, since they have reduced capacitance and longer transit times at a given bias voltage. The cells prepared at NREL were spin-coated using the procedures previously reported in ref.1. A scanning electron microscope (SEM) cross-sectional image is shown in Fig. SM-1. 0.13 cm^2 silver back contacts were used for these cells. The thickness of the perovskite absorber layer in this image matched the thickness obtained from voltage pulse capacitance measurements using the published relative permittivity ε_r = 18 for methylammonium lead iodide films.1 We have used DC-pulse capacitance measurements to confirm the actual perovskite layer thickness.

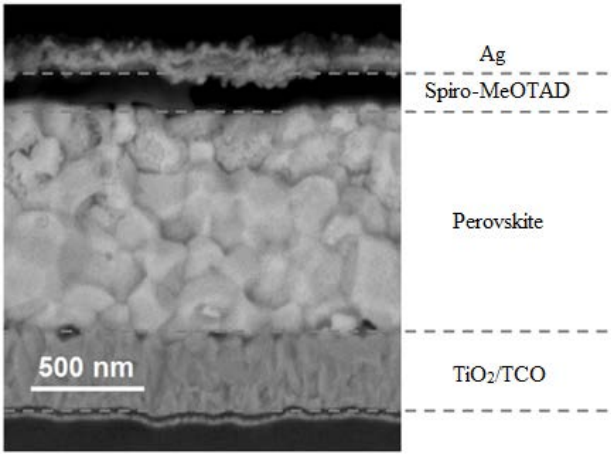

Fig. SM-1: Cross sectional image of a completed device from NREL using spin-coating.

The Iowa State samples were prepared using a sequential vapor deposition process described previously.[2] First, a requisite thickness of PbI_2 film was deposited followed by thermal anneal in a graphite crucible inside a nitrogen-filled glove box at 180 C in the presence of methylammonium iodide vapor. The thickness of the final perovskite layer is approximately twice the thickness of the deposited PbI_2 as determined using surface profilometry. Capacitance measurements on finished cells were again consistent with the physical thickness measurements.

Photo-current transients

When dispersive transport measurements were first analyzed in the 1970s,[3] it was found that a characteristic transit time t_T for photocarriers traversing a sample could be identified in logarithmic photo-current vs. time plots, which showed a "kink" between pre- and post-transit currents. The photocurrent $i(t)$ following a short impulse of light or electron excitation at time $t = 0$ can be written in the following form:

$$i(t) = \begin{cases} i_0(t/t_T)^{-1+\alpha}, t < t_T \\ i_0(t/t_T)^{-1-\alpha}, t \geq t_T \end{cases}, \quad \text{(SM-1)}$$

where $i_0 = \alpha Q_0/2t_T$, Q_0 is the complete photocharge collection at long times, and α is the dispersion parameter. In this Letter we have used the photocharge transients instead of photocurrent transients. For reference we show a transient photocurrent plot for sample I3B1 as Fig. SM-2. The post-transit decay agrees with the form of Eq. SM-1. The pre-transit form is affected by the *RC* risetime of the sample, where *C* is the microsecond domain capacitance of the sample and *R* is associated with the 50 ohm impedance of the cabling and electronics. The fact that the photocurrent reaches a maximum before *RC* is a consequence of the convolution of the *RC* response and the rapidly falling dispersive photocurrent.

The transit time kink is somewhat obscured in the figure. Under these conditions, we prefer to determine the transit time from the time for the integrated photocurrent to reach $Q_0/2$, which is a readily reproduced procedure that is independent of the transport model. When dispersive transport applies, previous work

has shown the photocharge procedure gives the same result as the kink. The dispersion parameter α from the post-transit decay in Fig. SM-2 agrees with that obtained with two alternate procedures in the Letter.[4]

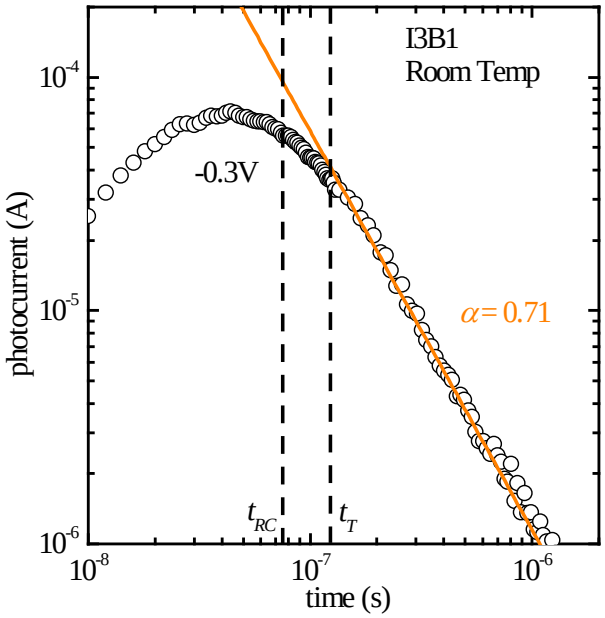

Fig. SM-2: Log-log photo-current transient for sample I3B1 at room temperature. The dispersion parameter, α, has the same value used for the photocharge transient and the drift-mobility fittings in Fig. 2 of the Letter. Here t_T = 107 ns and t_{RC} = 76 ns.

---

[1] Y. Zhou, M. Yang, W. Wu, A. L. Vasiliev, Kai Zhu, and N. P. Padture, J. Mater. Chem. A, 3, 8178 (2015).
[2] H. Abbas, R. Kottokkaran, M. Samiee, L. Zhang, B. Ganapathy, A. Kitahara, M. Noack, and V. L. Dalal, Appl. Phys. Lett. Mat. 3, 016105 (2015).
[3] H. Scher and E. Montroll, Phys. Rev. B 12, 2455 (1975).
[4] Q. Wang, H. Antoniadis, E. A. Schiff, and S. Guha, Phys. Rev. B 47, 9435 (1993).